Available online at www.sciencedirect.com
SCIENCE DIRECT®
Acta Materialia 53 (2005) 2509–2520
Acta MATERIALIA
www.actamat-journals.com

Atomic volumes and local structure of metallic glasses

I. Bakonyi *

Research Institute for Solid State Physics and Optics, Hungarian Academy of Sciences, P.O. Box 49, H-1525 Budapest, Hungary

Received 25 November 2004; received in revised form 9 February 2005; accepted 10 February 2005
Available online 2 April 2005

Abstract

The composition dependence of the room-temperature average atomic volume is analysed for early and late transition metal (TE–TL type) and metal–metalloid (TL–MD type) amorphous alloys. For the Zr–Cu, Ti–Cu and Hf–Ni sytems, the data suggest an ideal solid solution behaviour. For the other TE–TL systems, two composition ranges can be distinguished (20–70 at.% TL and 84–93 at.% TL). For each composition range, a specific atomic volume $V_{a\text{-}Zr}$ can be assigned to the Zr atoms that has the same value for any of the alloying components TL = Fe, Co and Ni. For TE-rich compositions (range 1), $V_{a1\text{-}Zr} \approx V_{hcp\text{-}Zr}$ whereas for TL-rich compositions (range 2), $V_{a2\text{-}Zr} < V_{a1\text{-}Zr}$. For the TL atoms, whereas both $V_{a2\text{-}TL}$(TE–TL) and $V_{a\text{-}TL}$(TL–MD) are fairly close to the V_{TL} values of the close-packed crystalline structures, the $V_{a2\text{-}TL}$(TE–TL) values are smaller by as much as about 2–3% than the $V_{a\text{-}TL}$(TL–MD) values.

Keywords: Density; Atomic volume; Amorphous alloys; Amorphous metals

1. Introduction

Many of the late transition metals (TL) such as Fe, Co, Ni, Pd, Pt and, in some cases, also Cu are well-known for their ability to form relatively easily glasses when alloyed with either metalloids (MD) such as B, P, C and Si or early transition metals (TE) such as Y, Sc, Ti, Zr, Hf, Mo and W. These metal–metalloid (TL–MD) and metal–metal (TE–TL) glasses can be considered as constituting two large classses of amorphous alloys. In recent decades, a vast amount of data have been accumulated on the properties of these amorphous alloy systems and it appears to be useful to perform a comparison and analysis of available data for some systematic alloy series with the aim of revealing common characteristics of that particular set of alloy families; this would then help to further deepen our understanding of the nature of structurally disordered alloys in general.

It is a particularly useful approach to consider a series of binary systems in a given amorphous alloy family and compare the properties of several binaries while varying one of the constituent elements (MD, TE or TL). As an example, we might mention the work of Shirakawa et al. [1] who studied and analysed the density and atomic volumes of TL–MD type metallic glasses, among others for the binary Fe–B, Fe–P, Co–B, Co–P and Ni–P systems. More recently, an analysis of specific heat and superconducting data has been performed [2] for some TE–TL type glasses including mainly the Ti–Cu, Ti–Ni, Zr–Cu and Zr–Ni binary systems, in order to establish systematic trends of the electronic density of states when varying either the alloy composition or the alloying element. By using the results of a theoretical study [3] of the electronic band structure of the different structural modifications of the early transition metals Ti, Zr and Hf, this investigation [2] has allowed also some conclusions to be drawn concerning the atomic structure of TE–TL glasses that was found to be strongly reminiscent of an face-centered cubic (fcc) like atomic arrangement. This conclusion is strongly supported by the previous finding

* Tel.: +36 13922628; fax: +36 13922215.
E-mail address: bakonyi@szfki.hu.

1359-6454/$30.00
doi:10.1016/j.actamat.2005.02.016

of a crystallization study [4] of $Zr_{67}Ni_{33}$ glasses according to which the very first crystallization product is indeed an fcc-Zr_2Ni structure.

The aim of the present work is to summarize available room-temperature density and atomic volume data for binary TE–TL glasses containing the elements TE = Ti, Zr and Hf, TL = Fe, Co, Ni and Cu, including data also for their binary stoichiometric crystalline compounds. We shall first review the atomic volume data for the individual TE and TL metals in their crystalline modifications as well as for the TL metals as deduced from TL–MD type glasses wherein the data of Shirakawa et al. [1] will be completed with the results of studies published since then.

It is believed that this work will provide a useful compilation of atomic volume data for both the TE–TL and TL–MD type glasses. Besides, an analysis of the dependence of atomic volume on alloy composition and alloying element in TE–TL glasses should shed some more light on our understanding of the local atomic structure in this class of amorphous alloys. The present paper is an extension of our previous work on the density and atomic volumes in TL-rich TE–TL glasses [5].

In view of the recently increased interest in bulk amorphous alloys which can in many cases be considered as TE–TL–MD type glasses, a combined discussion of atomic volume data for the TE–TL and TL–MD type amorphous alloys may be particularly useful.

2. Analysis of atomic volume data

For an amorphous alloy $A_{100-x}B_x$ where x denotes the composition of element B in at.%, the average atomic volume $V_{A\text{-}B}$ can be obtained from the measured density ρ by the expression

$$V_{A-B}[\text{Å}^3/\text{atom}] = 1.66 M_{A-B}[\text{g/mol}]/\rho[\text{g/cm}^3], \quad (1)$$

where $A = 6.02293 \times 10^{23}$ atom/vol for Avogadro's number and $M_{A\text{-}B}$ is the composition-averaged molar mass of the alloy.

For crystalline metals and alloys, V can be derived also from the measured lattice constants. For the fcc and body-centered cubic (bcc) structures with the lattice parameter a, as well as for the hexagonal close-packed (hcp) structure with the lattice parameters a and c, the corresponding atomic volumes are obtained as $V_{fcc} = a^3/4$, $V_{bcc} = a^3/2$ and $V_{hcp} = \sqrt{3}a^2c/4$.

The packing fraction is defined as

$$\eta = (4\pi/3)\langle R^3\rangle/V, \quad (2)$$

where R is an appropriately chosen effective atomic radius. For metals, it is customary to set R equal to the 12-fold-coordinated Goldschmidt atomic radius R_G. A few typical values are R_G(bcc-Fe) = 1.274 Å, R_G(hcp-Co) = 1.252 Å, R_G(fcc-Ni) = 1.246 Å, R_G(hcp-Zr) = 1.602 Å [6].

Since for amorphous alloys the density is derived directly from experiments, the composition dependence of this quantity has often been considered. On the other hand, as suggested by Turnbull [7] and adopted by, e.g., Shirakawa et al. [1] as well, an analysis in terms of atomic volumes is a physically more appropriate approach and we shall also follow this practice. As a reason in favour of this choice we may say that, even if it is also not an easy task to predict the composition dependence of the average atomic volume, at least we can assign a physical meaning to the data if the average atomic volume varies linearly, as is often the case, in a limited composition range. Namely, a linear composition dependence of V for a binary alloy system $A_{100-x}B_x$ can be described by the assumption that in this composition range atoms A and B have constant atomic volumes V_A and V_B, respectively, i.e., one can describe the data by the expression

$$V_{A-B} = (100 - x)V_A/100 + xV_B/100. \quad (3)$$

The simplest case of the composition dependence of the average atomic volume is when V varies linearly throughout the whole composition range of an alloy system A–B from pure A to pure B metal (Fig. 1). The atomic volumes V_A and V_B assigned to the two kinds of atoms in these alloys equal their corresponding values in the constituent pure metals. This behaviour can be considered as a manifestation of Vegard's law and an alloy of this type is termed as an ideal solid solution. Such a behaviour can be expected for crystalline alloys of two fairly similar metals which exhibit the same crystal structure and form a continuous series of solid solutions with this structure.

However, a more common behaviour, especially for crystalline alloys with components of significantly differ-

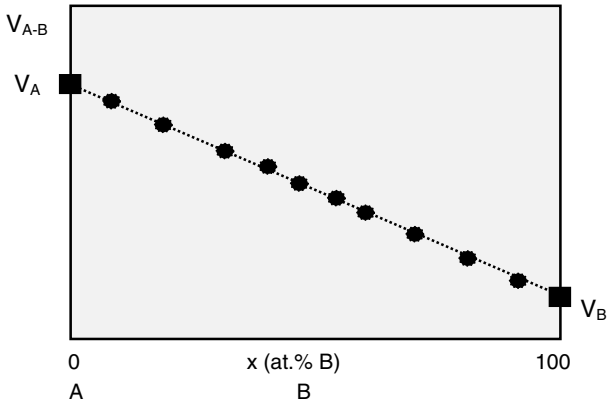

Fig. 1. Composition dependence of the average atomic volume $V_{A\text{-}B}$ in an ideal solid solution (single-phase alloy from A to B). Note: V_A and V_B mean the atomic volumes of atoms A and B in the pure metals A and B, respectively.

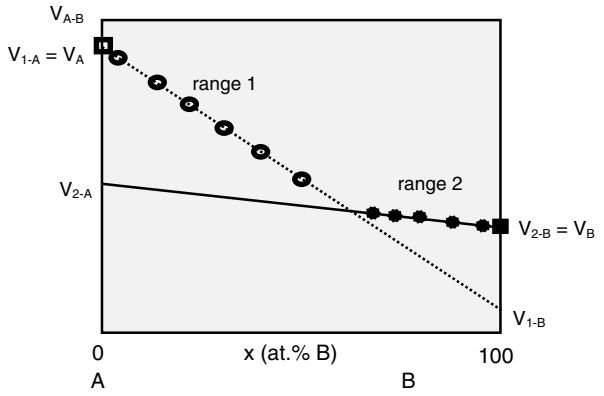

Fig. 2. Composition dependence of the average atomic volume $V_{A\text{-}B}$ in an alloy with two terminal solid solutions. Note: $V_{1\text{-}A}$ and $V_{1\text{-}B}$ mean the atomic volumes of atoms A and B, respectively, in composition range 1 (composition range extending from pure metal A), and the notation is similar for range 2.

ent atomic diameters and electronic structures, is that they form two terminal solid solutions (Fig. 2) over a limited concentration range which are of the form A(B) and B(A), eventually even with different crystal structures of the pure metals A and B, respectively. As pointed out by Turnbull [7], the atomic volume in such a case follows approximately a straight line when introducing metal B into A and metal A into B. However, the slopes are different for the two lines and this means that for A-rich compositions (composition range 1) we get $V_{1\text{-}A} = V_A$ and $V_{1\text{-}B} < V_B$ and for B-rich compositions (range 2), $V_{2\text{-}B} = V_B$ and $V_{2\text{-}A} < V_A$. Here V_A and V_B refer to the atomic volumes in the pure metals A and B, respectively. Similarly, $V_{1\text{-}A}$ and $V_{1\text{-}B}$ are the corresponding atomic volumes of A and B in range 1 and $V_{2\text{-}A}$ and $V_{2\text{-}B}$ are those in range 2.

Fig. 2 displays the scheme for an alloy system with negative deviation from Vegard's law. There may, however, also be a positive deviation that can be treated qualitatively in the same manner.

If an intermetallic compound phase also exists in the solid solution range, its atomic volume usually falls close to the solid solution straight line although does not necessarily fit exactly onto it, since for such specific compositions there may be special electronic structure effects which can result in an atomic volume different from that of the corresponding random solid solution alloys.

3. Atomic volumes of TE and TL metals and metalloids

3.1. Atomic volumes in the pure metals

3.1.1. Early transition metals (TE = Ti, Zr and Hf)

The stable form of Ti, Zr and Hf metals at room temperature is the hcp structure and their lattice constants [8] are summarized in Table 1 from which the atomic volumes $V_{lattice}$ were calculated. Table 1 also shows the available room temperature density data [9] which yielded the atomic volumes $V_{density}$.

Table 1
Lattice parameters (a and c) and density of Ti, Zr and Hf metals as well as the corresponding atomic volumes $V_{lattice}$ and $V_{density}$, respectively

Phase	Lattice parameters [8]		$V_{lattice}$ (Å^3/atom)	Density, ρ [9] (g/cm^3)	$V_{density}$ (Å^3/atom)
	a (Å)	c (Å)			
hcp-Ti	2.9508	4.6855	17.67	4.51	17.63
hcp-Zr	3.232	5.147	23.28	6.5	23.30
hcp-Hf	3.198	5.061	22.41	13.28	22.31

3.1.2. Late transition metals (TL = Fe, Co, Ni, Cu)

The room temperature lattice parameters [8] and density [9] of the stable crystalline modifications of Fe, Co, Ni and Cu metals are given in Table 2 together with the corresponding atomic volumes $V_{lattice}$ and $V_{density}$.

For the high temperature fcc phases of Fe and Co, the atomic volume and lattice parameter data reported in Ref. [10] (Fe and Co) and Ref. [11] (Fe) were used to plot the atomic volume as a function of temperature and to linearly extrapolate it to 20 °C. This procedure yielded the values included in the last two rows of Table 2.

It is noted that for both the TE and TL metals, the atomic volumes $V_{lattice}$ and $V_{density}$ of the room temperature stable modifications of each metal are in very good agreement with each other (see Tables 1 and 2), the relative difference being below 1% in each case, mostly even a few tenths of a per cent only. Since the lattice constant determinations are more accurate than the density measurements, we shall use the $V_{lattice}$ values in the following (by dropping the subscript "lattice").

The difference between the extrapolated room-temperature atomic volumes of the fcc-Co phase and the stable hcp-Co phase is similarly small (0.06%) whereas it is much larger (4%) when comparing room-temperature atomic volumes for the stable bcc-Fe phase and for the high-temperature fcc-Fe phase.

3.2. Atomic volumes of TL metals and metalloids in TL–MD glasses

Shirakawa et al. [1] presented an extensive compilation of density and atomic volume data for TL–MD glasses, specifically for the Fe–B, Fe–P, Co–B, Co–P and Ni–P systems. For each of the binaries considered, the composition dependence of the average atomic volume data could be fitted to straight lines. For the Co–B and Co–P systems, we accepted the fit values Shirakawa et al. [1] obtained from the available data whereas for Fe–B, the data sets were refitted which resulted in slightly different fit values. For the Fe–P and Ni–P systems, we have considered also density data published since then and the analysis was based on the

Table 2
Lattice parameters (a and c) and density of the different crystal structures of Fe, Co, Ni and Cu metals as well as the corresponding atomic volumes $V_{lattice}$ and $V_{density}$, respectively

Phase	Lattice parameters [8]		$V_{lattice}$ (Å^3/atom)	Density, ρ [9] (g/cm^3)	$V_{density}$ (Å^3/atom)
	a (Å)	c (Å)			
Stable room-temperature phases					
bcc-Fe	2.8665		11.78	7.86	11.79
hcp-Co	2.5071	4.0695	11.08	8.9	10.99
fcc-Ni	3.5232		10.93	8.9	10.95
fcc-Cu	3.6148		11.81	8.96	11.77
High-temperature phases extrapolated to room temperature (see text for details)					
fcc-Fe			11.38 [10,11]		
fcc-Co			11.14 [10]		

joint set of old and new data. Furthermore, we have also collected density data for the Ni–B system.

The fit results are collected in Table 3 by specifying the atomic volumes of the TL metals, $V_{a\text{-}TL}$(TL–MD), and the metalloids, V_{MD}, as deduced by fitting Eq. (3) to the available data. Below, we shall be mainly concerned with a discussion of the data reported after the work by Shirakawa et al. [1].

It is implied in Table 3 that the atomic volumes we can ascribe to Fe atoms in the amorphous Fe–B and Fe–P alloys are equal, i.e., $V_{a\text{-}Fe}$(Fe–B) = $V_{a\text{-}Fe}$(Fe–P). This value, $V_{a\text{-}Fe}$(Fe-MD) = 12.10 Å^3/atom, can also be considered as the atomic volume of Fe in hypothetical amorphous iron as derived from amorphous Fe-metalloid alloys. For these systems, the atomic volume data are visualized in Fig. 3 where the thick solid line sections cover the composition range over which data were reported by Shirakawa et al. [1], including both melt-quenched and electrodeposited alloys, and the dashed lines are extrapolations only (e.g., to pure amorphous Fe). Subsequently, Dietz and coworkers [12,13] reported an extensive set of atomic volume data (about 80 samples) for electrodeposited amorphous Fe–P alloys which fit rather well to the previous results although for lower Fe concentrations they may systematically lie somewhat below the fitted line of Shirakawa et al. [1]. For the sake of clarity, the results of Dietz and coworkers [12,13] are not reproduced in Fig. 3 but even if we included them into the evaluation, the Fe–B and Fe–P data could still be reasonably well fitted with the same Fe atomic volume, $V_{a\text{-}Fe}$(Fe-MD) = 12.10 Å^3/atom. The thick solid lines in Fig. 3 represent the fit with atomic volume data in Table 3.

Fig. 3 also shows the atomic volume of the compounds Fe_3B, Fe_2B, Fe_3P, Fe_2P [14] which are systematically smaller than those of the corresponding amorphous alloys. This can be ascribed to the "excess free volume" in the amorphous phase, occurring due to the topological disorder. It can also be seen in Fig. 3 that $V_{a\text{-}Fe}$(Fe-MD) > $V_{bcc\text{-}Fe}$ > $V_{fcc\text{-}Fe}$.

Nevertheless, we can conclude that the amorphous alloys and crystalline compounds follow the same trend of compositional dependence for a given metalloid species. Furthermore, the atomic packing in Fe–B alloys is much

Table 3
Parameters describing the composition dependence of the average atomic volume of amorphous TL_xMD_{100-x} alloys (TL = Fe, Co or Ni; MD = B or P) according to Eq. (3)

Alloy system	$V_{a\text{-}TL}$(TL–MD) (Å^3/atom)	For TL: $(V_{am} - V_{cr})/V_{cr}$ (%)	MD component		
			B	P	Si
			$V_{a\text{-}B}$ (Å^3/atom)	$V_{a\text{-}P}$ (Å^3/atom)	$V_{a\text{-}Si}$ (Å^3/atom)
Am. Fe-MD	12.10 (fcc: 11.38) (bcc: 11.78)	+6.3 +2.7	4.47	10.90	
Am. Co-MD	11.42 (fcc: 11.14) (hcp: 11.08)	+2.5 +3.1	4.43	9.90	
Am. Ni-MD	11.09 (fcc: 10.93)	+1.5	4.90	11.05	
Am. $(Mo_{0.6}Ru_{0.4})$-MD	15.33 (hcp: 14.61)	+4.9	3.93		10.97
Am. Pd–Cu-MD	14.33 (fcc: 13.62)	+5.2		11.76	

The data for the crystalline (bcc, fcc, hcp) structures of the TL metals are from Table 2. The data for the quasi-binary alloys in the last two rows are from Ref. [38].
Am.: amorphous.

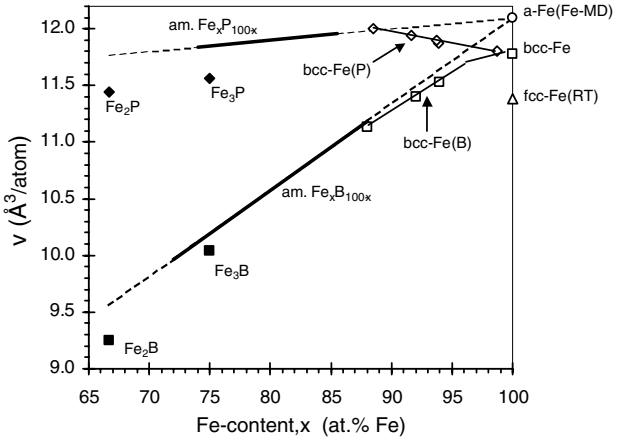

Fig. 3. Dependence of the room-temperature average atomic volume V on Fe-content x in amorphous and crystalline Fe-metalloid (Fe_xMD_{100-x}) alloys. The thick solid lines denote the fitted values for melt-quenched Fe–B and melt-quenched and electrodeposited Fe–P amorphous alloys in the composition range of available data according to the fit results in Table 3. The dashed lines are extrapolations of the thick lines to concentrations where no data are available in the amorphous state. Key to symbols: ○ (atomic volume of hypothetical amorphous iron, $V_{a\text{-}Fe}$(Fe-MD), extrapolated from amorphous Fe-MD alloys, see Table 3), ◆ (Fe_2P and Fe_3P [14]), ■ (Fe_2B and Fe_3B [14]), ◇ (bcc-Fe(P) solid solution alloys obtained by electrodeposition [13]), □ (bcc-Fe(B) solid solution alloys obtained by melt-quenching [15] and $V_{lattice}$ value for bcc-Fe from Table 2), Δ ($V_{lattice}$ value for fcc-Fe obtained by extrapolation to room temperature, see Table 2).

more efficient than in Fe–P alloys (see Fig. 3). The reason for this behaviour may lie in both the atomic size and chemical valence difference of P and B.

There are data available for electrodeposited bcc-Fe(P) [13] and melt-quenched bcc-Fe(B) [15] solid solution alloys which are also displayed in Fig. 3. These data join smoothly the value for bcc-Fe, indicating their solid solution behaviour. As for the amorphous alloys, the atomic volumes are higher also here for the Fe–P system than for Fe–B. With decreasing Fe content, the solid solution data approach the atomic volumes of the corresponding amorphous alloys. This might be connected partly with the fact that with increasing metalloid content, as was shown for the Fe(P) solid solutions [13], the crystallite size significantly decreases (down to 20 nm) and these alloys are actually nanocrystalline. On the other hand, smaller grain sizes enhance the solid solubility. The increase of the topological disorder with decreasing crystallite size is finally converted into an amorphous structure beyond a certain metalloid content.

The decrease of V in bcc-Fe(B) solid solutions was interpreted [15] by the substitution of 2 Fe atoms by 3 B atoms in the bcc lattice and this was supported by magnetic data as well. By replacing Fe atoms with the much smaller B atoms, a contraction of the lattice, i.e., a decrease of V is expected and observed. The fairly smooth transition of atomic volume data from the bcc-Fe(B) solid solutions to the amorphous Fe–B alloys suggests that this "substitutional" character of B atoms may be retained in the Fe–B metallic glasses as well.

On the other hand, the comparable size of Fe and P atoms, and also the different bonding character between Fe and P with respect to that between Fe and B, leads to an increase of V in the bcc-Fe(P) solid solutions with increasing P content. In these solid solutions, P also probably substitutionally enters the bcc lattice but, at the same time, the decrease in crystallite size introduces such an amount of lattice defects, mainly grain boundaries, that as a final effect, V may increase as observed. However, in the amorphous composition range, Fig. 3 shows that the increase of the P content reduces V, indicating a change in the substitutional character of P atoms towards a more efficient packing in the structurally disordered state in comparison with the nanocrystalline state.

The variation of the average atomic volume in the bcc-Fe(B) and bcc-Fe(P) alloys and especially the observed difference in the influences of B and P may certainly have a magnetic origin as well. By adding metalloid atoms to bcc-Fe, the band structure and, thus, the net magnetic moment certainly changes differently for the two metalloids due to their significantly different sizes and electronic configurations. On the other hand, magnetovolume effects, i.e., an interrelation between atomic volume and magnetic moment, are known to be significant in Fe-based alloys but the discussion of such subtle details is beyond the scope of the present paper.

The behaviour of the average atomic volume data for the Co–P and Co–B systems (Fig. 4) is qualitatively very similar to the results presented for the Fe-MD alloys. In addition to the data summarized by Shirakawa et al. [1], Dietz and Börngen [12] also reported an extensive set of density data (for clarity, not shown in Fig. 4) on electrodeposited Co–P amorphous alloys which properly fit to the results summarized in Ref. [1], represented by the thick solid line of Fig. 4 drawn according to the parameters of Table 3. The average atomic volume of amorphous cobalt $V_{a\text{-}Co}$(Co-MD) = 11.42 Å^3/atom as extrapolated from amorphous Co-MD alloys is slightly higher than the corresponding values of the close-packed crystalline modifications of Co as the data in Fig. 4 indicate.

The situation is more complicated for the Ni-MD alloys. This is mainly because some of the data for chemically reduced (electroless) Ni–P alloys do not completely fit into the corresponding data for the electrodeposited and melt-quenched Ni–P amorphous alloys. The average atomic volume data are shown in Fig. 5 for the Ni–P system. The results denoted by the symbols Δ have been reported for a mixture of fcc-Ni and Ni_3P phases obtained by annealing electrodeposited amorphous Ni–P alloys [16,17]. These data follow nicely

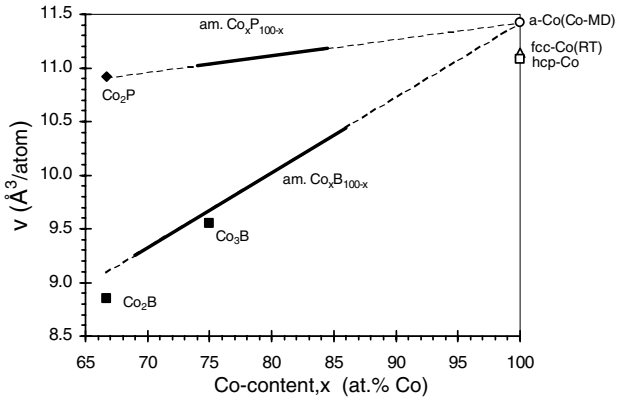

Fig. 4. Dependence of the room-temperature average atomic volume V on Co-content x in amorphous and crystalline Co-metalloid (Co-MD) alloys. The thick solid lines and the dashed lines have the same meaning as in Fig. 3. Key to symbols: ○ (atomic volume of hypothetical amorphous cobalt, $V_{a\text{-}Co}$(Co-MD), extrapolated from amorphous Co-MD alloys, see Table 3), ◆ (Co_2P [14]), ■ (Co_2B and Co_3B [14]), □ ($V_{lattice}$ value for hcp-Co from Table 2), Δ ($V_{lattice}$ value for fcc-Co obtained by extrapolation to room temperature, see Table 2).

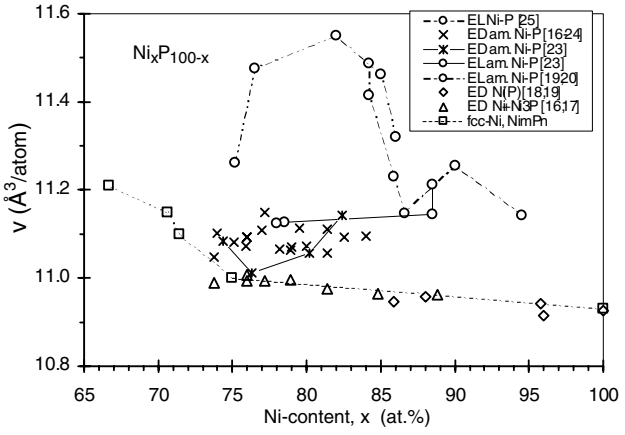

Fig. 5. Dependence of the room-temperature average atomic volume V on Ni-content x in amorphous and crystalline Ni–P alloys prepared by electrodeposition (ED) and electroless (EL) deposition and in crystalline stoichiometric Ni–P compounds. Key to symbols: × :electrodeposited amorphous Ni–P alloys [16–24] (data from Ref. [23] are connected by a solid line); ○: electroless deposited (mostly amorphous) Ni–P alloys (data connected by solid line: [23], data connected by double-dot-dashed line: [19,20], data connected by dash-dotted line: [25]); ◇: ED fcc-Ni(P) solid solution alloys [18,19]; Δ: phase mixture of fcc-Ni + Ni_3P obtained by heat treatment of electrodeposited amorphous Ni–P alloys [16,17]; □ (joined by dashed lines): fcc-Ni [8] and Ni_mP_n stoichiometric compounds [14,26–28].

the line joining the values for fcc-Ni and Ni_3P. It is interesting to note that the data (◇) for electrodeposited Ni(P) solid solution alloys [18,19] are also close to this trendline. On the other hand, these data also suggest that in the concentration range 85–100 at.% Ni, the introduction of P into the fcc-Ni lattice causes a much smaller increase of the average atomic volume than there was for bcc-Fe(P) (see Fig. 3). At lower Ni-contents (below 75 at.% Ni), the crystal structure of the Ni–P stoichiometric compounds becomes less densely packed and V increases more strongly [14,20]. The average atomic volume of electrodeposited Ni–P alloys [16–19,21–24] seems to be intermediate between the Ni_2P and Ni_3P phases, unlike the Fe–P system. The electrodeposited Ni–P alloy data in Fig. 5 suggest that the average atomic volume changes abruptly upon a transition from the Ni(P) solid solution phase to the amorphous state in the composition range around 85 at.% Ni.

The data for electroless Ni–P alloys denoted by circles (○) are presented separately in Fig. 5. The data points from the three independent investigations [19,23,25] are connected by different lines to distinguish them since they differ significantly from each other. Also, the structural state of these Ni–P alloys has not been thoroughly reported in each case. Based on the large average atomic volume values for the electroless Ni–P alloys in comparison with the results on the electrodeposited ones, a possible polymorphism of the amorphous state in Ni–P alloys was suggested [20] in the sense that different preparation techniques may result in different atomic arrangements of the amorphous state. However, the atomic volume data from the density measurements of Schmidt et al. [23] on electroless Ni–P alloys fit nicely into the trend for the electrodeposited and melt-quenched alloys (Figs. 5 and 6). Since their electrodeposited and melt-quenched Ni–P alloy data also fit into the other reported data, we consider their electroless density data as reliable. This implies that

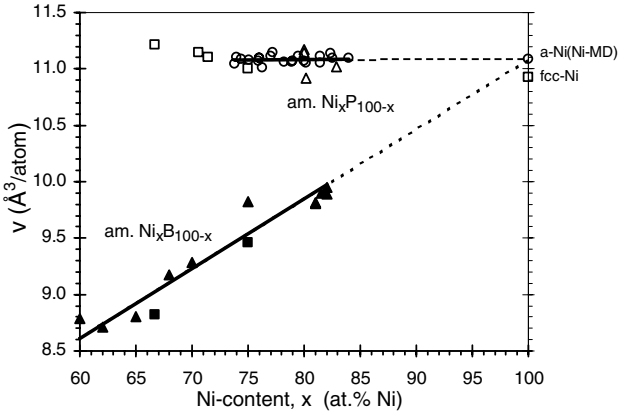

Fig. 6. Dependence of the room-temperature average atomic volume V on Ni-content x in amorphous and crystalline Ni-metalloid (Ni-MD) alloys. The thick solid lines and the dashed lines have the same meaning as in Fig. 3. Key to symbols: □: crystalline stoichiometric Ni_3P, Ni_5P_2, $Ni_{12}P_5$ and Ni_2P compounds [14,26–28] and $V_{lattice}$ value for fcc-Ni [8] from Table 2; ○: electrodeposited amorphous Ni–P alloys [16–24] (the same symbol is used for the atomic volume of hypothetical amorphous Ni, $V_{a\text{-}Ni}$(Ni-MD), extrapolated from amorphous Ni–P alloys, see Table 3); Δ: melt-quenched amorphous Ni–P alloys [23,30,31]; ●: melt-quenched amorphous Ni–B alloys [32–35]; ■: crystalline stoichiometric Ni_3B and Ni_2B compounds [14,26,36,37].

the electroless deposition technique does not necessarily result in different amorphous atomic arrangements than the other techniques (electrodeposition, melt-quenching), just that there are apparently still some unclear details of this particular preparation process [18,25]. Due to the discrepancy of the electroless data, we shall omit them from the further considerations. We have also omitted the large set of data by Dietz and Klein [29] for electrodeposited amorphous Ni–P alloys which were very close to the other data but exhibited a much larger scatter.

The average atomic volume data for the Ni–P and Ni–B system are summarized in Fig. 6 where data are included for electrodeposited [16–19,21–24] and melt-quenched [23,30,31] Ni–P alloys and for melt-quenched Ni–B amorphous alloys [32–35]. In Fig. 6, the upper thick solid line gives the fit to all electrodeposited and melt-quenched Ni–P amorphous alloys and the extrapolations are denoted by the dashed lines according to the atomic volume data in Table 3. As was the case for the Fe-MD and Co-MD alloy systems, we assume also here that $V_{\text{a-Ni}}$(Ni–B) = $V_{\text{a-Ni}}$(Ni–P) = 11.09 Å^3/atom and this yields for the Ni–B system the atomic volume of B as given in Table 3.

The value $V_{\text{a-Ni}}$(Ni-MD) = 11.09 Å^3/atom is somewhat smaller than that obtained by Shirakawa et al. [1] whose result was deduced from the Ni–P data of Ref. [16] only; here we used a much larger data set by including Ni–B alloys as well.

It can be seen in Table 3 that both $V_{\text{a-B}}$(TL–MD) and $V_{\text{a-P}}$(TL–MD) show a scatter by about 10% but it can still be established that $V_{\text{a-P}}$(TL–MD) $\approx 2\ V_{\text{a-B}}$(TL–MD). Similar data reported in Ref. [38] for two quasi-binary alloy series were also evaluated and the corresponding atomic volume data are listed in Table 3. As to the $V_{\text{a-TL}}$(TL–MD) values, they show also in these quasi-binary systems several per cent increase with respect to the atomic volumes in the corresponding close packed structures of the base alloys.

4. Atomic volumes in TE-TL glasses and intermetallic compounds

4.1. Composition range 1 (TL < 70 at.%)

The atomic volumes of Zr–Cu and Ti–Cu metallic glasses as well as some stoichiometeric intermetallic compounds are shown in Fig. 7. For fitting the data displayed in Fig. 7 by Eq. (3), we assumed that the atomic volume of Cu in both systems equals $V_{\text{fcc-Cu}}$ and the atomic volumes of Ti and Zr are equal to the values in their close packed stable structure, i.e., $V_{\text{hcp-Ti}}$ and $V_{\text{hcp-Zr}}$, respectively. The fitted lines indicate that this assumption is justified. The atomic volumes from these fits are given in Table 4. Fitting the data without any fixed parameter resulted in very close values for both the TE and Cu atoms and the fit quality improved only slightly.

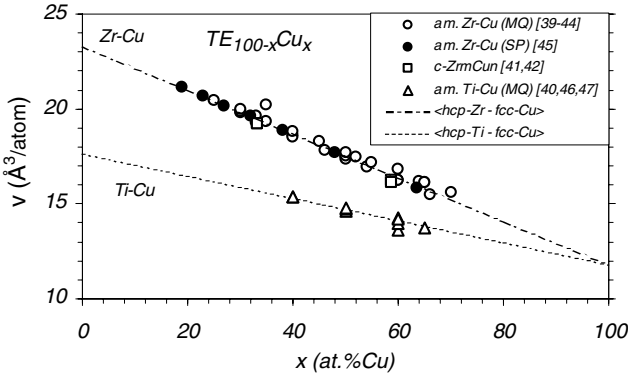

Fig. 7. Dependence of the room-temperature average atomic volume V on Cu-content x in amorphous and crystalline $TE_{100-x}Cu_x$ alloys for TE = Ti and Zr (see Refs. [39–47]). The dash-dotted and dashed lines represent Vegard's law for Zr–Cu and Ti–Cu alloys, respectively, by using atomic volumes of the corresponding close-packed structures of the constituent metals (see Table 4).

According to the discussion in Section 2, from the fact that all the atomic volume data can be described by straight lines, we can assign a constant atomic volume for each alloy constituent over the whole composition range of available data. Since these atomic volume values are equal to the corresponding values in the close-packed structures of the pure metals, both the Zr–Cu and Ti–Cu systems can be identified as forming an ideal solid solution in the amorphous state. (As argued in Section 1 and in Ref. [2], the amorphous state can be considered as reminiscent of an fcc-like local structure; however, since the atomic volume is practically the same for the two close-packed structures (fcc and hcp) as evident for Co in Table 2, we can also take $V_{\text{hcp-Ti,Zr}} = V_{\text{fcc-Ti,Zr}}$.)

This behaviour may be connected with the fact that the Cu atoms have a closed 3d-shell which lies well below the Fermi level where the electronic density of states is dominated by the TE atom d-bands. Therefore, the Cu atoms may have a relatively weak bonding with the TE atoms and this can lead to a random atomic arrangement in the TE–Cu amorphous alloys without a chemical short-range order (CSRO). According to the theoretical calculations of Nguyen-Manh et al. [48], amorphous Zr–Cu alloys do not exhibit any CSRO.

The atomic volume data for amorphous Zr–Ni alloys and stoichiometric compounds are shown in Fig. 8. The data can be well fitted by Eq. (3) with the assumption of $V_{\text{a1-Zr}} = V_{\text{hcp-Zr}}$ and the resulting $V_{\text{a1-Ni(Zr)}}$ value is given in Table 4. The dashed line in Fig. 8 indicates Vegard's law from which it follows that $V_{\text{a1-Ni(Zr)}} < V_{\text{fcc-Ni}}$.

The atomic volume data for amorphous Hf–Ni alloys are shown in Fig. 9. The data lie fairly close to Vegard's law, i.e., we can take in this case $V_{\text{a1-Ni(Hf)}} = V_{\text{fcc-Ni}}$. This means that the amorphous Hf–Ni system in the

Table 4
Parameters describing the composition dependence of the average atomic volume V of amorphous TE–TL alloys (TE = Ti, Zr or Hf; TL = Fe, Co or Ni) according to Eq. (3)

	V (Å^3/atom)	V (Å^3/atom) [$(V_{am} - V_{cr})/V_{cr}$]		
TL metal	(close packed TL structures)	$V_{a1\text{-}TL}$(TE–TL)	$V_{a2\text{-}TL}$(TE–TL)	$V_{a\text{-}TL}$(TL–MD)
Fe	11.38 (fcc)	10.51 (Zr) [−7.6%]	11.78 (Zr) [+3.5%]	12.10 [+6.3%]
Co	11.14 (fcc) 11.08 (hcp)	9.72 (Zr) [−12.7%]	11.17 (Zr) [+0.3%]	11.42 [+2.5%]
Ni	10.93 (fcc)	10.01 (Zr) [−8.4%] 10.93 (Hf) [0%]	≈10.85 (Zr) [−0.7%]	11.09 [+1.5%]
TE metal	(close packed TE structures)	$V_{a1\text{-}TE}$(TE–TL)	$V_{a2\text{-}TE}$(TE–TL)	
Ti	17.67 (hcp)			–
Zr	23.28 (hcp)	23.28 (Fe, Co,Ni)	21.50 (Fe, Co,Ni) [−7.6%]	–
Hf	22.41 (hcp)	22.41 (Ni)		–
TE metal	(close packed TE structures)	$V_{a\text{-}TE}$(TE–Cu)		$V_{a\text{-}Cu}$(TE–Cu) ($V_{fcc\text{-}Cu}$ = 11.81)
Ti	17.67 (hcp)	17.67		11.81
Zr	23.28 (hcp)	23.28		11.81

For comparison, the values of the close packed (fcc, hcp) structures from Tables 1 and 2 and the values $V_{a\text{-}TL}$(TL–MD) from Table 3 are also given. At the bottom, similar data are included for the Ti–Cu and Zr–Cu amorphous alloys. The values in bracket [ ] after the atomic volume data indicate the relative deviation with respect to the corresponding close-packed values.

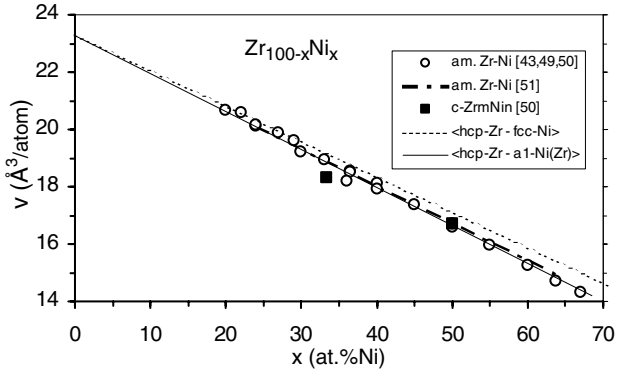

Fig. 8. Dependence of the room-temperature average atomic volume V on Ni-content x in amorphous and crystalline $Zr_{100-x}Ni_x$ alloys (see Refs. [43,49–51]). The dashed line represents Vegard's law by using atomic volumes of the corresponding close-packed structures of the constituent metals. The solid line represents a fit to the data by Eq. (3) whereby fixing the atomic volume of Zr atoms as equal to $V_{hcp\text{-}Zr}$. The fitted value of the Ni atomic volume is given in Table 4.

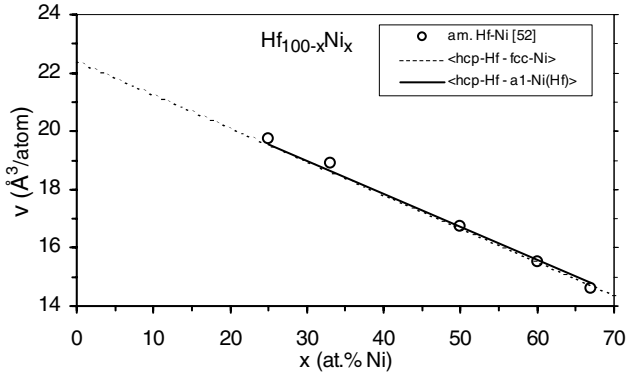

Fig. 9. Dependence of the room-temperature average atomic volume V on Ni-content x in amorphous $Hf_{100-x}Ni_x$ alloys (see Ref. [52]). The dashed line represents Vegard's law by using atomic volumes of the corresponding close-packed structures of the constituent metals (see Table 4). The solid line represents a fit to the data by Eq. (3) whereby fixing the atomic volume of Hf atoms as equal to $V_{hcp\text{-}Hf}$. The fitted value of the Ni atomic volume was practically equal to $V_{fcc\text{-}Ni}$.

composition range from 25 to 67 at.% Ni also behaves as an ideal solid solution.

The atomic volume data for amorphous Zr–Co (Fig. 10) and Zr–Fe (Fig. 11) alloys can be fitted by Eq. (3) in a similar way as was the case for the amorphous Zr–Ni system: $V_{a1\text{-}Zr} = V_{hcp\text{-}Zr}$ and all the data show a negative deviation from Vegard's law. The fitted values of $V_{a1\text{-}Co(Zr)}$ and $V_{a1\text{-}Fe(Zr)}$ are specified in Table 4.

It can be established from Table 4 that the $V_{a1\text{-}TL}$(TE–TL) values are all much smaller than the atomic volumes of the corresponding crystalline TL metals. This indicates that in the amorphous state the TL atoms are packed more space-efficiently in the skeleton of the large TE atoms than in the corresponding close-packed fcc-TL structures, i.e., a negative deviation from Vegard's law occurs in composition range 1.

The different behaviour of the Zr-TL alloys (TL = Fe, Co, Ni) in comparison with the TE–Cu alloys (TE = Ti, Zr), i.e., the presence or absence of a deviation from Vegard's law, respectively, may originate from the unfilled d-bands of the TL metals which lie higher in energy than the Cu 3d bands. All this results in stronger bonds via more effective hybridization between the Zr 4d and TL 3d bands. The stronger bonds, on the other hand, can

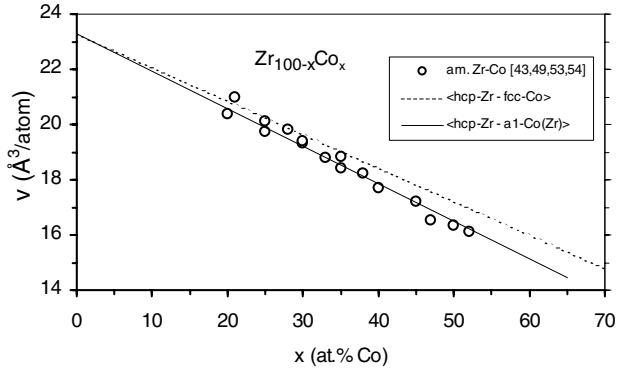

Fig. 10. Dependence of the room-temperature average atomic volume V on Co-content x in amorphous $Zr_{100-x}Co_x$ alloys (see Refs. [43,49,53,54]). The dashed line represents Vegard's law by using atomic volumes of the corresponding close-packed structures of the constituent metals. The solid line represents a fit to the data by Eq. (3) whereby fixing the atomic volume of Zr atoms as equal to $V_{hcp\text{-}Zr}$. The fitted value of the Co atomic volume is given in Table 4.

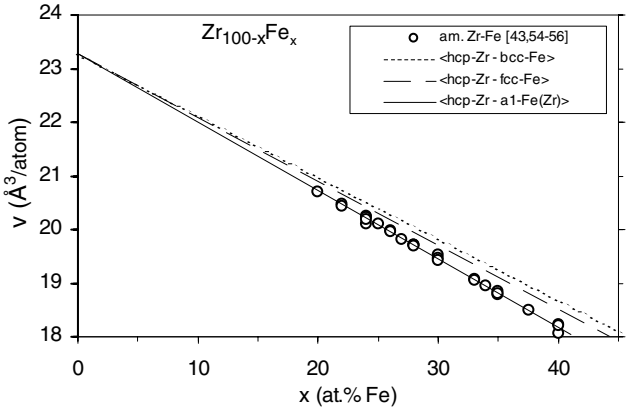

Fig. 11. Dependence of the room-temperature average atomic volume V on Fe-content x in amorphous $Zr_{100-x}Fe_x$ alloys (see Refs. [43,54–56]). The short-dashed and long-dashed lines represent Vegard's law by using atomic volumes of the bcc-Fe and fcc-Fe, respectively, in both cases with hcp-Zr atomic volume. The solid line represents a fit to the data by Eq. (3) whereby fixing the atomic volume of Zr atoms as equal to $V_{hcp\text{-}Zr}$. The fitted value of the Fe atomic volume is given in Table 4.

lead to the development of a CSRO. According to the theoretical work by Nguyen-Manh et al. [48], an increasing CSRO develops in the Zr–Ni system for higher Ni contents: whereas in a-$Zr_{65}Ni_{35}$ there is almost no CSRO, a clear CSRO develops in a-$Zr_{50}Ni_{50}$ and the CSRO is even stronger in a-$Zr_{35}Ni_{65}$. The increasing CSRO means a larger preference for unlike atom first neighbourhood. All these considerations are well in line with the observed increasing deviation from Vegard's law for higher Ni contents.

4.2. Composition range 2 ($TL \approx 90$ at.%)

The atomic volume data for amorphous Zr-TL (TL = Fe, Co, Ni) alloys for compositions around 90 at.% TL content were presented and analysed in a previous work [5]. The data for these amorphous alloy systems were fitted by Eq. (3) under the constraint that $V_{a2\text{-}Zr}$ should be the same for each of the TL metals (Fe, Co, Ni). The fitted values of $V_{a2\text{-}Zr}$ and $V_{a2\text{-}TL}$(TE–TL) are given in Table 4 and Fig. 12 shows the fits for the whole composition range.

To visualize the large difference between the atomic volumes in composition ranges 1 and 2 for both the TE and TL constituents, all the Zr–Fe data are displayed in Fig. 13 together with fitted lines over the whole

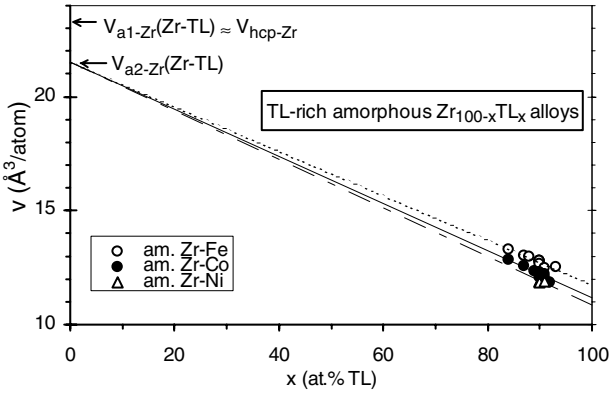

Fig. 12. Dependence of the room-temperature average atomic volume V on TL-content x in amorphous $Zr_{100-x}TL_x$ alloys with TL = Fe, Co and Ni. The experimental data are from Ref. [5] and the lines through the data points are least-square fits according to Eq. (3) to the data with the fit paramaters ($V_{a2\text{-}Zr}$ and V_{TL}) given in Table 4. When performing the fits, it was assumed that $V_{a2\text{-}Zr}$ has the same value for all three TL metals.

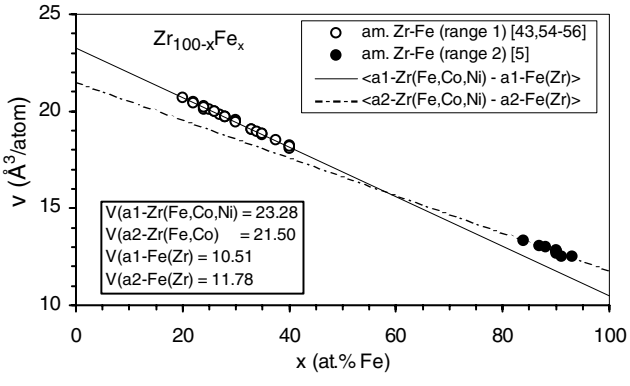

Fig. 13. Dependence of the room-temperature average atomic volume V on Fe-content x in amorphous $Zr_{100-x}Fe_x$ alloys for the whole composition range (see Refs. [5,43,54–56]). The lines through the data points are least-square fits according to Eq. (3) to the data with the fit parameters as indicated (see also Table 4).

composition range. Evidently, $V_{a2\text{-}Zr}$ is significantly smaller than $V_{a1\text{-}Zr} = V_{hcp\text{-}Zr}$. Furthermore, we can see that $V_{a1\text{-}Fe}(TE–TL) < V_{a2\text{-}Fe}(TE–TL)$. The same relations hold true for the other two TL elements (Co and Ni) as well.

4.3. Other TE-based amorphous alloys

One can extend the above analysis to results on quasi-binary alloys. Fig. 14 shows data for the (Zr–Ti)–Ni and (Zr–Nb)–Ni systems [49]. The lines were obtained by scaling down the atomic volume $V_{a1\text{-}Zr(Ni)}$ in Table 4 to the composition $Zr_{78}Ni_{22}$ and by assuming that $V_{a1\text{-}Ni(Ti)} = V_{a1\text{-}Ni(Nb)} = V_{a1\text{-}Ni(Zr)}$, the latter value given in Table 4 and by taking the available atomic volume for Nb ($V_{bcc\text{-}Nb}$ = 17.97 Å^3/atom [8]). These lines match quite well the experimental data apart from a small systematic difference that arises due to the fact that in Ref. [49] the measured value for a-$Zr_{78}Ni_{22}$ is somewhat above the average data (see Fig. 8) from which the fit parameters in Table 4 were deduced.

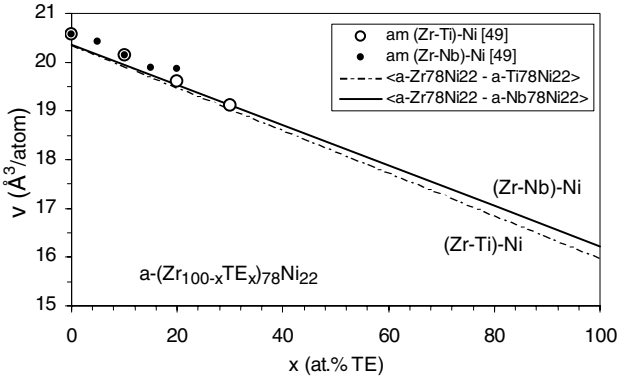

Fig. 14. Dependence of the room-temperature average atomic volume V on TE-content x in amorphous $(Zr_{100-x}TE_x)_{78}Ni_{22}$ alloys for TE = Ti and Nb (see Ref. [49]). The lines were obtained as described in the text.

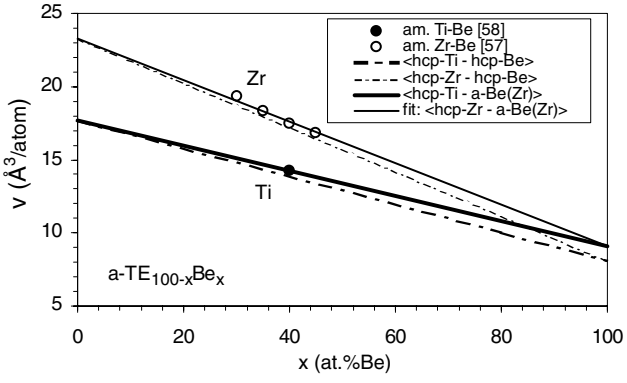

Fig. 15. Dependence of the room-temperature average atomic volume V on Be-content x in amorphous $TE_{100-x}Be_x$ alloys for TE = Ti and Zr (see Refs. [57] and [58]) . The lines were obtained as described in the text.

There are some data also for amorphous Zr–Be [57] and Ti–Be [58] alloys (Fig. 15). The amorphous Zr–Be data were fitted (thin solid line) by using $V_{a\text{-}Zr} = V_{hcp\text{-}Zr}$ which then yielded $V_{a\text{-}Be(Zr)}$ = 9.10 Å^3/atom. By taking this $V_{a\text{-}Be(Zr)}$ value and $V_{a\text{-}Ti} = V_{hcp\text{-}Ti}$, the thick solid line was drawn which goes nicely through the only amorphous Ti–Be data point. The thin and thick dash-dot lines indicate Vegard's law for the Zr–Be and Zr–Ti systems, respectively, with $V_{hcp\text{-}Be}$ = 8.11 Å^3/atom [8]. These data indicate that the Zr–Be and Zr–Ti amorphous alloy data can be well fitted by using a common value for hypothetical amorphous Be. The experimental data exhibit a positive deviation from Vegard's law for these Be-containing alloys in contrast to the TE–TL alloy systems where either no or negative deviation was observed.

5. Summary

In the present work, available atomic volume data derived from published densities were presented for TL–MD and TE–TL type amorphous alloys. In most cases, a linear variation of the average atomic volume with alloy composition was obtained. From an analysis of the atomic volume data, the atomic volumes assignable to the individual alloy constituents were derived. The main conclusions of the present study can be summarized as follows.

(a) TL–MD amorphous alloys
  (i) Fo r a given TL metal (Fe, Co or Ni), the TL-P and TL-B amorphous alloy atomic volume data could be separately fitted by a straight line with a common value for the hypothetical amorphous TL metal ($V_{a\text{-}TL}$). For each TL metal, the $V_{a\text{-}TL}$ values were slightly above the corresponding $V_{fcc\text{-}TL}$ values, the difference amounting to a few per cent (Table 3).
  (ii) Although the B and P atomic volumes derived exhibited a scatter of about 10% for the three TL elements, the $V_{a\text{-}P}$ values were about twice as large as the $V_{a\text{-}B}$ values.
  (iii) For Fe and Co, the P atomic volume is by about 10% smaller than $V_{a\text{-}Fe}$ and $V_{a\text{-}Co}$ whereas for Ni, it was established that $V_{a\text{-}P} \approx V_{a\text{-}Ni}$. In view of item (ii), this also implies that in these metallic glasses B occupies typically half a volume than the matrix TL metal atoms.

(b) TE–TL amorphous alloys
  (i) For Zr–Cu and Ti–Cu, the atomic volume data indicate an ideal solid solution behaviour in that the atomic volumes assignable to the individual alloy constituents are equal to the values in the

corresponding close-packed structures. This is the fcc structure for Cu and hcp for Ti and Zr. However, since the atomic packing efficiency is practically the same for the fcc and hcp structures (see Table 2 for Co), one can consider also the values for fcc-Zr and fcc-Ti as being equal to the $V_{a\text{-}Zr}$ and $V_{a\text{-}Ti}$ data, respectively, in these systems. An ideal solid solution behaviour was obtained also for the Hf–Ni system.

(ii) For the other TE–TL systems with TE = Zr and TL = Fe, Co and Ni, two compositon ranges had to be distinguished to describe the atomic volume data: range 1 for TL < 70 at.% and range 2 for TL ≈ 90 at.%. In this situation, the data could be analysed by considering two terminal solid solutions.

(iii) For the Zr-TL alloys (TL = Cu, Fe, Co and Ni), the difference in the atomic volume behaviour between Cu and the other three metals (Fe, Co and Ni) could be ascribed to the different bonding characters between Zr and Cu and between Zr and TL = Fe, Co or Ni. These considerations were supported by theoretical band structure calculations [48] which established a difference in the degree of CSRO for the Zr–Cu and Zr–Ni systems.

(iv) In composition range 1, the atomic volume data could be well described by using $V_{a1\text{-}Zr} = V_{hcp\text{-}Zr}$ for all three TL metals whereas the $V_{a1\text{-}TL}$ values were 8–13% smaller than the corresponding $V_{fcc\text{-}TL}$ values.

(v) In composition range 2, the $V_{a\text{-}Zr}$ value was 7.6% below the close-packed value for Zr whereas the $V_{a2\text{-}TL}$ values were quite close to the corresponding TL close-packed values.

(c) Comparison of TL atomic volumes as deduced from TL–MD and TE–TL amorphous alloys.

(i) For each TL metal, the $V_{a2\text{-}TL}$(TE–TL) value is slightly but systematically below the corresponding $V_{a\text{-}TL}$(TL–MD) value. This can be taken as an indication that there may exist two slightly different amorphous phases of each of these TL metals.

(ii) This observation provides a support for a previous conclusion by Xiao and Chien [59], obtained from magnetic measurements for the two distinct states of amorphous Fe.

(iii) The atomic volume data for Fe also provide a basis for explaining the "normal" ferromagnetic behaviour of Fe-MD glasses as opposed to the "abnormal" magnetic behaviour manifesting itself in a complicated magnetic phase diagram for amorphous Zr–Fe alloys. For the latter, this has already been partly discussed in Ref. [5] and further details along these lines will be published elsewhere [60].

It should be finally noted that there has been recently a report on the preparation of an amorphous phase of pure Zr metal [61]. There were already attempts [2,62] to deduce some physical properties of amorphous Zr. It is hoped that the present work also provides data which can give further insight into the characteristics of pure amorphous Zr metal.

Acknowledgements

This work has been supported by the Hungarian Scientific Research Fund (OTKA) through grant No. T 034 666. In the early stage of this work, the author has benefited from discussions with Z. Altounian. A careful reading of the manuscript by R. Hasegawa is also acknowledged.

References

[1] Shirakawa K, Waseda Y, Masumoto T. Sci Rep RITU (Sendai) A 1981;29:229.
[2] Bakonyi I. J Non-Cryst Solids 1995;180:131.
[3] Bakonyi I, Ebert H, Liechtenstein AI. Phys Rev B 1993;48:7841.
[4] Brauer S, Strom-Olsen JO, Sutton M, Yang YS, Zaluska A, Stephenson GB, et al. Phys Rev B 1992;45:7704.
[5] Bakonyi I, Kisdi-Koszó É, Altounian Z. Mater Sci Eng A 1997;226–228:641.
[6] Pearson WB. The crystal chemistry and physics of metals and alloys (Wiley-Interscience, New York, USA, 1972). The 12-coordinated metallic radii in Table 4-4 of this book have been taken from: Teatum E, Gschneidner K, Waber J. Report LA-2345 (US Department of Commerce, Washington, DC, USA, 1960).
[7] Turnbull D. Scripta Metall 1977;11:1131;
Turnbull D. Scripta Metall 1981;15:1039;
Turnbull D. Acta Metall Mater 1990;38:243.
[8] Villars P, Calvert LD. Pearson's handbook of crystallographic data for intermetallic phases. Metals Park, OH: American Society of Metals; 1985.
[9] Landolt-Börnstein. The structure data of the elements and intermetallic phases. New Series, vol. III/6. Berlin: Springer Verlag; 1971. pp. 1–40.
[10] Kohlhaas R, Dünner Ph, Schmitz-Pranghe N. Z Angew Phys 1967;23:245.
[11] Chaudron G, editor. Monographies sur les Métaux de Haute Pureté, vol. 1. Paris: Masson et Cie; 1972. [chapter 11].
[12] Dietz G, Börngen L. J Non-Cryst Solids 1983;58:275.
[13] Dietz G, Richter K, Stein F, Schäfer HC. Z Phys B – Cond Matter 1990;81:223.
[14] Chen HS. Acta Metall 1976;24:153.
[15] Ray R, Hasegawa R. Solid State Commun 1978;27:471.
[16] Cargill III GS. J Appl Phys 1970;41:12.
[17] Logan J, Ashby MF. Acta Metall 1974;22:1047.
[18] Brenner A, Couch DE, Williams EK. J Res NBS 1950;44:109.
[19] Gustafson PS. Ph.D Thesis, College of William and Mary, Williamsburg, VA, 1981.
[20] Lashmore DS, Bennett LH, Schone HE, Gustafson P, Watson RE. Phys Rev Lett 1982;48:1760.
[21] Bagley BG, Turnbull D. J Appl Phys 1968;39:5681.
[22] Waseda Y, Miller WA. Phys Stat Sol (a) 1978;49:K31.
[23] Schmidt T, Varga L, Kemény T, Konczos G, Tompa K, Kajcsos Zs. Nucl Instrum Meth 1982;199:359.

[24] Dietz G, Schneider HD. J Phys: Cond Matter 1990;2:2169.
[25] Safranek WH. The properties of electrodeposited metals and alloys. New York: American Elsevier Publishing Co.; 1974.
[26] Samsonov GV, Vinitskii IM, editors. Handbook of refractory compounds. New York: IFI/Plenum; 1980.
[27] Saini GS, Calvert LD, Taylor JB. Can J Chem 1964;42:1511.
[28] Larsson E. Ark Kemi 1965;23:335.
[29] Dietz G, Klein F-J. J Non-Cryst Solids 1987;89:290.
[30] Davis LA, Chou CP, Tanner LE, Ray R. Scripta Metall 1976;10:973.
[31] Waseda Y, Masumoto T. Sci Rep RITU A 1978;27:21.
[32] Lamparter P, Nold E, Rainer-Harbach G, Grallath E, Steeb S. Z Naturforsch A 1981;36:165.
[33] Lamparter P, Sperl W, Steeb S, Bletry J. Z Naturforsch A 1982;37:1223.
[34] Waseda Y, Chen HS. Phys Stat Sol (a) 1978;49:387.
[35] Hasegawa R. US Patent No. 4,338,131, 1982.
[36] Rundqvist S, Pramatus S. Acta Chem Scand 1967;21:191.
[37] Lugscheider E, Reimann H. Z Metallkde 1980;71:239.
[38] Johnson WL, Williams AR. Phys Rev B 1979;20:1640.
[39] Chen HS, Waseda Y. Phys Stat Sol (a) 1979;51:593.
[40] Hake RR, Karkut MG, Aryainejad S. Physica B 1981;107:503.
[41] Calvayrac Y, Chevalier JP, Harmelin M, Quivy A, Bigot J. Philos Mag B 1983;48:323.
[42] Altounian Z, Tu GH, Strom-Olsen JO. J Appl Phys 1982;53:4755.
[43] Altounian Z, Strom-Olsen JO. Phys Rev B 1983;27:4149.
[44] Davis LA, Chou CP, Tanner LE, Ray R. Scripta Metall 1976;10:937.
[45] Zougmore F, Lasjaunias JC, Bethoux O. J Phys (Paris) 1989;50:1241.
[46] Mizutani U, Akutsu N, Mizoguchi T. J Phys F 1983;13:2127.
[47] Linqvist P, Rapp O. J Phys F 1988;18:1979.
[48] Nguyen-Manh D, Mayou D, Cyrot-Lackmann F, Pasturel A. J Phys F 1987;17:1309.
[49] Karkut MG, Hake RR. Phys Rev B 1983;28:1396.
[50] Bhatnagar AK, Rhie KW, Naugle DG, Wolfenden A, Zhang BH, Callway TO, et al. J Phys: Cond Matter 1990;2:2625.
[51] Dong YD, Gregan G, Scott MG. J Non-Cryst Solids 1981;43:403.
[52] Rathnayaka KDD, Rhie K, Hennings BD, Naugle DG. J Phys: Cond Matter 1993;5:7251.
[53] Altounian Z, Shank RJ, Strom-Olsen JO. J Appl Phys 1985;58:1192.
[54] Karkut MG, Hake RR. Physica B 1982;109–110:2033.
[55] Altounian Z, Volkert CA, Strom-Olsen JO. J Appl Phys 1985;57:1777.
[56] Krebs HU, Freyhardt HC. In: Steeb S, Warlimont H, editors. Rapidly quenched metals. Amsterdam: Elsevier Science Publishers B.V.; 1985. p. 439.
[57] Hasegawa R, Tanner LE. Phys Rev B 1977;16:3825.
[58] Davis LA, Chou CP, Tanner LE, Ray R. Scripta Metall 1976;10:937.
[59] Xiao G, Chien CL. Phys Rev B 1987;35:8763.
[60] Bakonyi I. Unpublished.
[61] Zhang JZ, Zhao YS. Nature 2004;430:332.
[62] Ristic R, Babic E, Fizika A., in press.